Journal of The Electrochemical Society, **157** (8) A953-A956 (2010)
0013-4651/2010/157(8)/A953/4/$28.00 © The Electrochemical Society

Lithium–Air Batteries Using SWNT/CNF Buckypapers as Air Electrodes

G. Q. Zhang,[a] J. P. Zheng,[a,c,z] R. Liang,[b,d] C. Zhang,[b,d] B. Wang,[b,d] M. Hendrickson,[e] and E. J. Plichta[e]

[a]*Department of Electrical and Computer Engineering and* [b]*Department of Industrial and Manufacturing Engineering, Florida A&M University and Florida State University, Tallahassee, Florida 32310, USA*
[c]*Center for Advanced Power Systems and* [d]*High Performance Materials Institute, Florida State University, Tallahassee, Florida 32310, USA*
[e]*U.S. Army Power Division, Army CERDEC, Fort Monmouth, New Jersey 07703, USA*

Li–air cells based on Li foil as an anode electrode, freestanding carbon nanotube/nanofiber mixed buckypaper as an air (cathode) electrode, and organic electrolyte were assembled. The air electrode was made with single-wall carbon nanotube (SWNT) and carbon nanofiber (CNF) without any binder. The discharge capacity was strongly dependent on both the discharge current density and the thickness of the air electrode. A discharge capacity as high as 2500 mAh/g was obtained for an air electrode at a thickness of 20 μm with a discharge current density of 0.1 mA/cm^2; however, it was reduced to 400 mAh/g when the thickness of the air electrode was increased to 220 μm. For a 66 μm thick air electrode, the discharge capacity decreased from 1600 to 340 mAh/g when the discharge current density increased from 0.1 to 0.5 mA/cm^2. The scanning electron microscope images on surfaces of the air electrode from a fully discharged cell showed that the voids at the air side were almost fully filled by the solid deposition; however, the voids at the membrane side were still wide open.
 [DOI: 10.1149/1.3446852]

Manuscript submitted April 12, 2010; revised manuscript received May 11, 2010. Published June 11, 2010.

The rapid growth of portable electronic devices has driven a need for high energy density storage devices. Recently, lithium (Li)–air batteries have been attracting much attention due to its extremely high specific capacity.[1-5] The reason for such high specific capacity is that there is a Li sheet as an anode electrode and a cathodic reactant of O_2 from the air. The theoretical maximum capacity of Li–air batteries is determined by the complete electrochemical oxidation of the metallic Li anode. The theoretical specific capacity of Li is 3862 mAh/g,[2,6] which is at least 1 order of magnitude higher than that of any types of electrode materials used in advanced Li-ion or Li-polymer batteries. Considering the high operational voltages 2.9–3.1 V for systems using nonaqueous electrolyte,[2] the theoretical maximum energy densities of Li–air batteries have been calculated based on charge balance and are 2790 Wh/kg and 2800 Wh/L in nonaqueous electrolytes and 1300–1400 Wh/kg and 1520–1680 Wh/L in duel electrolytes (nonaqueous in anode and aqueous in the cathode side);[7] this is not only much higher than that of any advanced batteries[8] but also higher than that of fuel cells.[9]

Although the theoretical energy density of Li–air batteries is extremely large, the practical discharge capacity and energy density of Li–air batteries are always cathode-limited due to the deposition of discharge products in the air electrode. From previous studies of air electrode made with Super P carbon in propylene carbonate (PC):dimethyl carbonate electrolyte at different discharge current conditions, at high discharge rates, a Li_2O_2/Li_2O discharge product deposited on the air side of the electrode, causing pore size and volume reducing, which limits O_2 access to the inner carbon black.[3] The reason for the increase in discharge products depositing near the air side of the electrode is because the O_2 concentration is higher closest to the oxygen side of the electrode.[2,4] In addition to the discharge products, which limit the maximum capacity of the battery, the O_2 concentration and reduction reaction rate in the electrode as well as electrical conductivity of the electrode limits the maximum current density of the battery.

Air electrode formulation has been an essential factor in determining the discharge capacity of metal–air batteries. In this paper, we wish to report a new air electrode based on integrated carbon nanotube (CNT) papers in Li–air batteries to replace conventional carbon blacks. The advantages of buckypapers include tailorable porosity, large surface area, and high conducting (100–500 S/cm) as well as potentially eliminating chemical containment such as catalysts during the CNT formation.[10]

Experimental

The single-wall carbon nanotube (SWNT)/CNT buckypapers were prepared using the filtration method. The detailed processes were described in a previous published article.[11,12] Briefly, SWNT/CNT buckypaper was produced by filtrating dimethylformamide suspension of SWNT (Carbon Nanotechnologies, Inc.) and CNT (Applied Sciences, Inc.) at a mixing ratio of 1:3 w/w. The diameter and length for the CNT were 0.8–1.2 and 100–1000 nm, respectively, and those for the carbon nanofiber (CNF) were 100–200 and 30–100 μm, respectively. The air electrode was taken directly by cutting the above prepared buckypaper to an active size of 2 cm in diameter. No binder was used during the buckypaper formation process.

The Li–air cells were designed to be oxygen electrode limited. The test cells were constructed in an argon atmosphere glove box. The cell mainly consisted of three parts. The air (cathode) electrode was made with a piece of buckypaper alone with a nickel mesh as the current collector. The anode electrode was made with a lithium (Li) foil (Sigma Aldrich, 99.9%, 0.38 mm thickness) and with the same size as the buckypaper electrode. The nonaqueous electrolyte was made with 1 M $LiPF_6$ (Sigma Aldrich, 99.99%) in PC (Sigma Aldrich, anhydrous 99.97%)/tetrahydrofuran (THF) (Sigma Aldrich, anhydrous 99.99%) at a ratio of 1:1 by weight. The buckypaper cathode and Li foil anode electrode were separated by a porous Cegard2400 film.

The pore size distribution of the buckypaper was measured using a surface analyzer (Micromeritics TriStar 3000). The cell was gastight except for the buckypaper electrode window exposed to oxygen atmosphere. Electrochemical measurements were carried out in 1 atm oxygen gas at room temperature using a Gamry instrument controlled by a computer. The resulting data were analyzed by the Gamry Echem Analyst program. The morphologies of the buckypaper electrode before and after discharge were characterized using a scanning electron microscope (SEM, JSM-7401, JEOL).

Results and Discussion

Figure 1 shows the pore size distribution of the buckypaper. From experimental results, the Brunauer, Emmett, and Teller surface area is 173 m^2/g, and the average pore width is 9.0 nm. A sharp

[z] E-mail: zheng@eng.fsu.edu

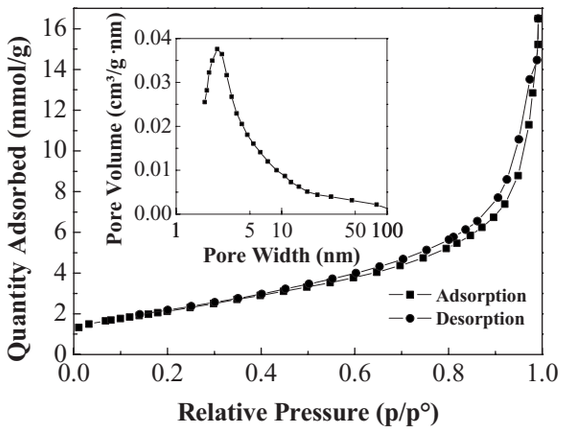

Figure 1. N_2 adsorption (squares)–desorption (circles) isotherm curves measured on buckypaper. The inset shows the corresponding BJH pore size distribution curve.

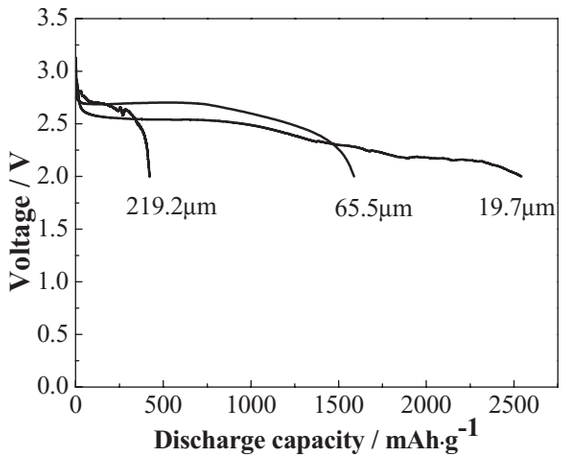

Figure 3. Discharge curves from Li–air cells made with different thicknesses under a constant current density of 0.1 mA/cm^2.

maximum at 3.4 nm, the pore size distribution curve (Fig. 1 inset) indicates the presence of mesopores of all diameters between 2 and 20 nm. The porosity of the buckypaper was estimated using simple algebra based on the weight and dimension measurements of the buckypaper and the mass density of bulk graphite (2.267 g/cm^3) and is about 77%. Figure 2 shows the SEM surface images of the buckypaper. The SWNTs and CNFs are entangled together to ensure good mechanical properties. The buckypaper was confirmed as a promising material for producing high strength composite. From our previous study, gas diffusivity increased with an increase in the weight ratio between CNF and SWNT; however, the pure CNF buckypaper is hard to prepare because of a lack of entanglement.

The electrical conductivity of the buckypaper was also measured using the standard electrical four-probe method and was ~17.4 S/cm. The electrical conductivity of the buckypaper increased by increasing the ratio of SWNT and CNF due to the highly conductive nature of the SWNT.

Figure 3 shows air electrode thickness dependence of discharge curves for Li–air cells made with Li foil (anode)/$LiPF_6$ in PC:THF/buckypaper (cathode/air). One side of the cathode electrode is exposed to 1 atm oxygen gas. The discharge capacity of the air electrode strongly depends on the thickness of the air electrode. The specific capacity was calculated based on the weight of CNT/SWNT buckypaper only. The maximum theoretical capacity for an air electrode at 77% porosity was estimated at 3398 mAh/g by assuming that all porous volume in the air electrode was filled by Li_2O_2 product after being fully discharged.[7] From Fig. 3, for a thin air electrode at 20 μm, the specific capacity of 2550 mAh/g was obtained at a discharge current density of 0.1 mA/cm^2; however, it decreased rapidly to ~1580 and 350 mAh/g when the thicknesses of the electrode increased to 66 and 220 μm, respectively.

The specific capacity of air electrode was also strongly dependent on the discharge current density, as shown in Fig. 4. Li–air cells were discharged at constant current densities of 0.1, 0.2, and 0.5 mA/cm^2. The air electrode thickness was 66 μm.

Discharge processes, as shown in Fig. 3 and 4, can be divided into three regions: (*i*) the cell voltage had a rapid drop during the initial discharge; (*ii*) the cell voltage decreased continuously during the entire discharge process; and (*iii*) the cell voltage drop accelerated during the last discharge process. The discharge processes can be explained by an electrochemical reaction rate equation and the oxygen concentration inside the air electrode and can be expressed as[4,13,14]

$$R(x) = \kappa\varepsilon(x)c_{O_2}(x)\left[\exp\left(\frac{0.5F}{RT}\eta\right) - \exp\left(-\frac{0.5F}{RT}\eta\right)\right] \quad [1]$$

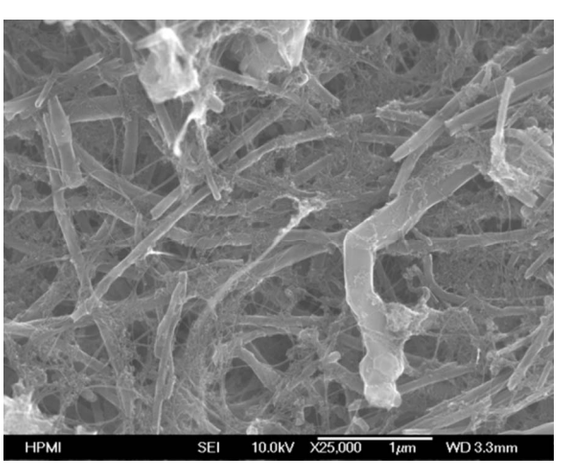

Figure 2. SEM image of a buckypaper surface.

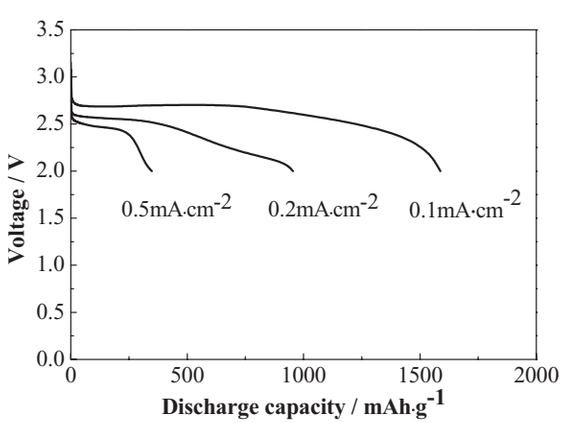

Figure 4. Discharge curves from Li–air cells at constant current densities of 0.1, 0.2, and 0.5 mA/cm^2.

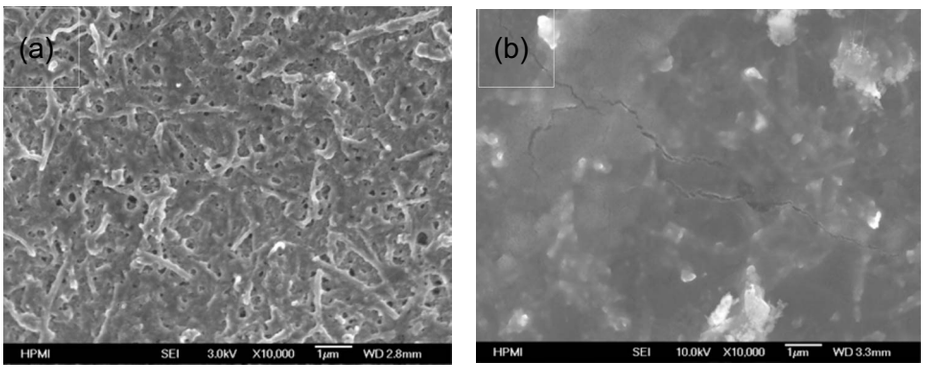

Figure 5. SEM images of the air electrode surfaces at (a) separator and (b) air sides after discharge at 0.1 mA/cm^2.

$$c_{O_2}(x) = c^0_{O_2} \exp\left(-\frac{Ax}{D_{O_2,\text{eff}}}\right) \quad [2]$$

where κ is a parameter that is proportional to the reaction rate coefficient, $\varepsilon(x)$ is porosity inside the air electrode, F is Faraday's constant, R is the universal gas constant, T is the absolute temperature, η is the electrode overpotential, $c^0_{O_2}$ is the oxygen concentration in air electrode at the air electrode/air interface, A is the parameter that is proportional to the current density, x is the depth from the air electrode/air interface into the air electrode, and $D_{O_2,\text{eff}}$ is the oxygen effective diffusion coefficient. Therefore, the oxygen diffusion length can be approximately described as $D_{O_2,\text{eff}}/A$. When the electrode overpotential is greater than $2RT/F$, the electrochemical reaction rate equation can be simplified as

$$R(x) = \kappa\varepsilon(x)c_{O_2}(x)\exp\left(\frac{0.5F}{RT}\eta\right) \quad [3]$$

Before the initial discharge, the initial oxygen concentration in the electrolyte was under the equilibrium state, which was determined by the oxygen pressure outside the air electrode and the solubility of the solvent used for the electrolyte; however, when the discharge started, oxygen inside the air electrode was depleted and a new equilibrium oxygen concentration was reached according to Eq. 2. The initial oxygen inside the air electrode was just enough to sustain a small discharge capacity at ~2.6 mAh/g, which was calculated based on the assumption of the external oxygen concentration of 1 atm, the solubility factor[6] of electrolyte of 0.0345, and electrode porosity of 77%. After this initial discharge, the oxygen concentration inside the air electrode reduced to a new equilibrium state described by Eq. 2, and $c_{O_2}(x)$ inside the air electrode was significantly lower than the initial concentration of $c^0_{O_2}$. To maintain a constant current discharge (or constant reaction rate), the overpotential must be significantly increased according to Eq. 3. That is why the initial voltage dropped, as shown in Fig. 3 and 4, and can be explained by the oxygen concentration rapid depletion inside the air electrode after the Li–air cell started to be discharged.

During the discharge, the oxygen concentration is not uniform inside the air electrode; the electrochemical reaction rate is also not uniform according to Eq. 3, which results in a nonuniform deposition rate of the Li_2O_2/Li_2O discharge product as well as the porosity inside the air electrode. More specifically, the porosity near the air side decreased faster than that close to the membrane side. The voltage decrease during the discharge in Fig. 3 and 4 can be explained as the porosity of the air electrode and oxygen concentration inside the air electrode decreased continuously; therefore, the overpotential of the cell must be continuously increased to maintain a constant reaction rate, as shown in Eq. 3.

At near the end of discharge, the porosity of the air electrode at the air side was close to zero. The oxygen diffusion channel was closed out (pinch-off) and the oxygen concentration inside the air electrode dropped rapidly. Because both porosity and oxygen concentration decreased, the overpotential must increase rapidly to maintain a constant reaction rate, as shown in Eq. 3; therefore, the cell voltage decreased rapidly, as shown in both Fig. 3 and 4. The important characteristic of Li–air cells is that the discharge products such as Li_2O_2/Li_2O are deposited within the oxygen diffusion depth from the air electrode/air interface. The deposition rate even within the oxygen diffusion depth could be very nonuniform. Figure 5 shows SEM images from two different surfaces of an air electrode (66 μm thick) after fully discharged at current density of 0.1 mA/cm^2. A clear difference of surface morphologies was observed at the air and membrane sides of the buckypaper air electrode. The surface at the air side was covered almost completely by the discharge product; however, the surface at the membrane side still had clear open pores.

The electrode thickness dependence of specific capacity as shown in Fig. 3 can be understood by the fact that the discharge product was deposited near the air electrode/air interface and within the oxygen diffusion length. When the thickness of the air electrode was greater than the oxygen diffusion length, most of the pore volume was not filled by the discharged product even though the cell was fully discharged; therefore, the specific capacity decreased.

The discharge current density dependence, as shown in Fig. 4, is because the oxygen diffusion length decreased with increasing discharge current density, as described by Eq. 2; therefore, at a higher discharge current density, the discharge products would deposit in a thinner layer near the electrode surface, which resulted in a lower specific capacity.

Electrochemical impedance spectra (EIS) for a Li–air cell with buckypaper air electrode were also recorded before and after discharge in the frequency range of 0.1–10^6 Hz. As seen in Fig. 6, the Nyquist plots display obviously similar shapes but very different sizes, suggesting different characteristics. A simple equivalent electric circuit was used to simulate the EIS, as shown in the inset of Fig. 6. In the circuit, the high frequency intercept of the semicircle on the real axis was reflected by an ohmic resistance (R_s), which includes ionic resistance from the separator paper and electrical resistance from both electrodes, current collectors, and the contact resistance between the electrode and the current collector. The depressed semicircle at middle frequency was contributed by a parallel combination of charge-transfer resistance (R_{ct}), which corresponds to the kinetic reaction at the air electrode surface, and a constant phase element (Z_Q), which corresponds to the double-layer capacitance at the porous air electrode surface. The linear spike at low frequency could be described by a finite length Warbury element (Z_W) arising from a diffusion-controlled process.

Mathematically, the constant phase element is given by

$$Z_Q = \frac{1}{Q_o(j\omega)^\alpha} \quad [4]$$

The factor α is less than 1. When α = 1, it becomes an ideal double-layer capacitance and value $Q_o = C$.

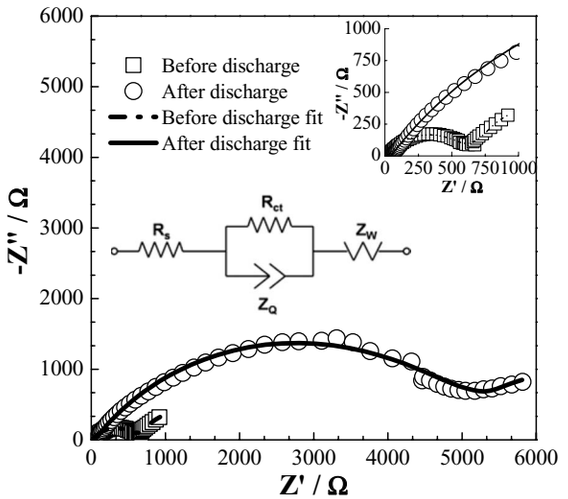

Figure 6. Electrochemical impedance spectrum of Li–air cell based on buckypaper air electrode before and after discharge at 0.1 mA/cm^2. The inset is the equivalent electric circuit used to fit EIS.

The governing equation for the finite length Warbury element can be expressed in terms of the distributed impedance of a transmission line containing three parameters with well-defined physical meaning and is given by

$$Z_W = R_W \frac{\tanh(\sqrt{j\omega\tau_d})}{\sqrt{j\omega\tau_d}} \quad [5]$$

Here, R_W is the ionic impedance of the porous electrode, $\tau_d = l^2/D$ is the diffusion time constant with D as the diffusion coefficient, l is the length of the diffusion region in the electrode, and ω (in rad/s) is the angular frequency.

Table I summarized all fitting parameters used to fit the EIS from a Li–air cell before and after discharge. Both ohmic and charge-transfer resistances increased significantly, particularly, the value of charge-transfer resistance increased by almost an order of magnitude. The increase in R_s resulted from the production of insulating solid discharge products Li_2O_2/Li_2O after discharge. Another possibility for increasing R_s is that the contact resistance between the electrode and current collector and the interfacial resistance between the electrolyte and electrode increased due to the volumetric change of the Li–air cell before and after discharge. The theoretical calculation shows that the volume of Li–air cell can decrease 23% after discharge.[7] The increase in R_{ct} is believed to be mainly due to the oxygen deficiency in the air electrode because of the pinch-off of the diffusion channel at the air side after discharge. The charge-transfer resistance is inversely proportional to the exchange current density and varies in proportion to the oxygen concentration inside the air electrode. EIS changes are consistent with the observation from SEM images of the surface morphology, which are obtained from the air electrode before and after discharge.

Table I. Fitted parameters in equivalent electric circuit.

			Z_Q		Z_W	
Parameter	R_s (Ω)	R_{ct} (Ω)	Q_o ($\Omega^{-1} - s^{\alpha}$)	α	R_W (Ω)	τ_d (s)
Before discharge	23.5	578	2.87×10^{-5}	0.64	868	34.9
After discharge	54.3	5093	3.10×10^{-5}	0.59	741	43.3

Conclusions

A Li–air cell made with SWNT/CNF air electrode can deliver a specific capacity as high as 2540 mAh/g at 0.1 mA/cm^2 discharge current density. The discharge capacity decreased with increasing thickness of air electrode and discharge current density. The SEM images clearly show that discharge products deposited nonuniformly inside the air electrode. The oxygen diffusion channel was pinched-off first at the electrode surface at the air side. It is believed that the specific capacity can be improved by using an air electrode having a porosity with a gradient. The high porosity at air side "delays" the pinch-off.

Acknowledgments

This work was supported by U.S. Army-CERDEC.

Florida A&M University and Florida State University assisted in meeting the publication costs of this article.

References

1. K. M. Abraham and Z. Jiang, *J. Electrochem. Soc.*, **143**, 1 (1996).
2. I. Kowalczk, J. Read, and M. Salomon, *Pure Appl. Chem.*, **79**, 851 (2007).
3. J. Read, *J. Electrochem. Soc.*, **149**, A1190 (2002).
4. J. Read, K. Mutolo, M. Ervin, W. Behl, J. Wolfenstine, A. Driedger, and D. Foster, *J. Electrochem. Soc.*, **150**, A1351 (2003).
5. T. Kuboki, T. Okuyama, T. Ohsaki, and N. Takami, *J. Power Sources*, **146**, 766 (2005).
6. D. Linden, *Handbook of Batteries*, 2nd ed.,McGraw-Hill, New York (1995).
7. J. P. Zheng, R. Y. Liang, M. Hendrickson, and E. J. Plichta, *J. Electrochem. Soc.*, **155**, A432 (2008).
8. H. Ibrahim, A. Ilinca, and J. Perron, *Renewable Sustainable Energy Rev.*, **12**, 1221 (2008).
9. D. N. Prater and J. J. Rusek, *Appl. Energy*, **74**, 135 (2003).
10. B. Wang, Z. Liang, B. Wang, and C. Zhang, *Adv. Mater.*, **19**, 1257 (2007).
11. W. Zhu, J. P. Zheng, R. Liang, B. Wang, C. Zhang, G. Au, and E. J. Plichta, *J. Electrochem. Soc.*, **156**, B1099 (2009).
12. W. Zhu, D. Ku, J. P. Zheng, R. Liang, B. Wang, C. Zhang, S. Walsh, G. Au, and E. J. Plichta, *Electrochim. Acta*, **55**, 2555 (2010).
13. C. O. Laoire, S. Mukerjee, K. M. Abraham, E. J. Plichta, and M. A. Hendrickson, *J. Phys. Chem. C*, **113**, 20127 (2009).
14. S. S. Sandhu, J. P. Fellner, and G. W. Brutchen, *J. Power Sources*, **164**, 365 (2007).